RSC Advances

PAPER

View Article Online
View Journal | View Issue

Cite this: *RSC Adv.*, 2023, **13**, 464

Synthesis, spectroscopic, SC-XRD/DFT and non-linear optical (NLO) properties of chromene derivatives†

Nadia Arif,[a] Zahid Shafiq, *[a] Sajida Noureen,[b] Muhammad Khalid, *[cd] Abida Ashraf,[a] Muhammad Yaqub,[a] Shabana Irshad,[cd] Muhammad Usman Khan,[e] Muhammad Nadeem Arshad,[f] Ataualpa Albert Carmo Braga,[g] Ahmed H. Ragab[h] and Saedah R. Al-Mhyawi[i]

In the present study, we reported the efficient synthesis of novel, heterocyclic, coumarin-based pyrano-chromene derivatives, 2-amino-8-methyl-5-oxo-4-[2-(2-oxo-2*H*-chromen-3-ylmethoxy)-phenyl]-4*H*,5*H*-pyrano[3,2-*c*]chromene-3-carbonitrile (**4a**) and 2-amino-8-methyl-5-oxo-4-[2-(2-oxo-2*H*-chromen-3-ylmethoxy)-phenyl]-4*H*,5*H*-pyrano[3,2-*c*]chromene-3-carboxylic acid methyl ester (**4b**). The chemical structures of synthesized compounds were resolved by employing various spectroscopic techniques like UV-Vis, FT-IR, ^{1}H & ^{13}C NMR, and single crystal X-ray diffraction (SC-XRD) analysis. The compounds; **4a** and **4b**, with appealing π-bonded skeleton were further analyzed in terms of their electronic and structural aspects using an integral approach of density functional theory (DFT) and time-dependent DFT (TD/DFT). The methodology: M06-2X/6-31G(d,p) level of theory was applied to compare their experimental data with theoretical outcomes using quantum chemical analysis. The frontier molecular orbitals (FMOs) study revealed that, **4a** possesses a low band gap (5.168 eV) as compared to **4b** (6.308 eV). Global reactivity parameters were associated with E_{gap} values as **4a**, with the lowest band gap showed the smaller value of hardness (0.094 eV) and a larger value of softness (5.266 eV). The non-linear optical (NLO) insight exhibited that, the average polarizability $\langle\alpha\rangle$ and second hyperpolarizability (γ_{tot}) were observed in **4a** as 6.77005 × 10^{-23} and 0.145 × 10^{4} esu, respectively. Overall, the computational studies suggest that the investigated compounds have distinct NLO properties.

Received 10th November 2022
Accepted 9th December 2022

DOI: 10.1039/d2ra07134g

rsc.li/rsc-advances

1. Introduction

Diversity-oriented synthesis of heterocyclic frameworks has become indispensable in the construction of novel fused ring heterocyclic compounds and thus aims to design natural product ring systems with useful pharmacophores for drug development.[1] The structural and activity profiles of various coumarin derivatives have inspired pharmaceutical chemists to develop new drugs with safe activity and selectivity in their action for a variety of therapeutic disorders.[2–5] Coumarin derivatives are well known for their critical role in the prevention and treatment of pathogenic and infectious diseases.[6,7] Coumarin-based analogues are intended to show discrete valuable biological and clinical activities vulnerable to substitution patterns exhibited by the parent benzopyran core.[8,9] Amongst the highly studied pharmaceutical activities, it is noteworthy for antibacterial,[10,11] antiviral,[12] antifungal,[13] anti-cancer,[14] anti-inflammatory,[15] antitubercular,[16] antioxidant,[17] antimutagenic,[18] anticoagulant,[19] scavenging of reactive oxygen species (ROS),[20] cyclooxygenase,[21] lipoxygenase,[22] cholinesterase

[a]*Institute of Chemical Sciences, Organic Chemistry Division, Bahauddin Zakariya University, Multan-60800, Pakistan. E-mail: zahidshafiq25@hotmail.com*
[b]*Materials Chemistry Laboratory, Institute of Chemistry, The Islamia University of Bahawalpur, 63100, Pakistan*
[c]*Institute of Chemistry, Khwaja Fareed University of Engineering & Information Technology, Rahim Yar Khan, 64200, Pakistan. E-mail: khalid@iq.usp.br; muhammad.khalid@kfueit.edu.pk*
[d]*Centre for Theoretical and Computational Research, Khwaja Fareed University of Engineering & Information Technology, Rahim Yar Khan, 64200, Pakistan*
[e]*Department of Chemistry, University of Okara, Okara-56300, Pakistan*
[f]*Center of Excellence for Advanced Materials Research (CEAMR), Faculty of Science, King Abdulaziz University, Jeddah, Saudi Arabia*
[g]*Departamento de Química Fundamental, Instituto de Química, Universidade de São Paulo, Av. Prof. Lineu Prestes 748, São Paulo, 05508-000, Brazil*
[h]*Department of Chemistry, Faculty of Science, King Khalid University, Abha 62224, Saudi Arabia*
[i]*Department of Chemistry, College of Science, University of Jeddah, Jeddah 21419, Saudi Arabia*

† Electronic supplementary information (ESI) available. CCDC 2115636–2115638. For ESI and crystallographic data in CIF or other electronic format see DOI: https://doi.org/10.1039/d2ra07134g

(ChE), and monoamine oxidase (MAO) inhibitory activities, vasodilator,[23] CNS stimulant,[24] and cytotoxic[25] potential.

The analysis of supramolecular architecture has greatly revolutionized research in the field of crystal engineering, which accommodates non-covalent interactions where molecules accumulate in self-assembly, possessing various inter and intramolecular interactions.[26,27] The strong interactions like hydrogen bonding (inter and intramolecular) also play a pivotal role in molecular biology, supramolecular frameworks and crystal engineering.[28,29] There are various structural diversities found in the heterocyclic frameworks, like the presence of electronegative groups (such as –F), which influence the molecular stability as well as the molecular level interactions with the biological receptors. The various privileged biological compounds that undergo structural diversities are found with enhanced efficiencies. Moreover, the rapid synthesis of wide-ranged heterocyclic compounds with the help of multi-component reaction techniques has attracted the attention of researchers.[30,31]

The heterocyclic chromene-based ring compounds are an important class of benzopyran family compounds that are efficiently being used in several pharmacological industries as antibacterial,[32–34] antiviral,[35] anti-malaria,[36] anti-inflammatory,[37] anti-cancer,[38] anti-HIV,[39] antifungal,[40] anti-anaphylactic, and anti-proliferative.[41] Computational analysis, also known as density functional (DFT) analysis, is an important method for predicting structural parameters such as non-covalent interactions, electronic properties, stability, and chemical reactivity.[42] The DFT and time-dependent DFT approaches envisage the bond distances, bond angles, FMOs, global reactivity descriptors (GRDs), natural population analysis (NPA), NBOs, molecular electrostatic potential (MEP), statistical average of molecular dipoles moment, linear and non-linear polarizabilities for various crystalline and non-crystalline compounds, including hydrazones, organic co-crystals,[43,44] pyrimidine rings[45] *etc.*

Non-linear optics (NLO) is one of the significant research areas which are being focused nowadays. In the present investigation, the chromene-based synthesized compounds are deliberated for their NLO parameters, *i.e.*, $\langle\alpha\rangle$, β_{tot}, and γ_{tot}, which were not evaluated so far, as evident from the literature review. Such organic compounds having a π-conjugated framework are efficiently utilized in wide bandwidth optical switching devices. The unique properties of such compounds as intramolecular charge transfer (ICT), electron delocalization, polarizability, and hyperpolarizability have paved the way for new research into efficient NLO devices.[46]

The chromene-based synthesized crystalline compounds, *i.e.*, **4a** and **4b**, were studied *via* the DFT approach. The NLO study of the entitled compounds might not be reported yet. Hence, to overcome the research gap, computational analysis is carried out to examine NLO properties. This research paper would be a new addition to the advancement of NLO compounds and surely serve as a synthesized non-fullerene (NF) based crystalline organic NLO materials in the research discipline for the future.

2. Experimental section

2.1 Synthesis of coumarin-based pyrano-chromene derivatives (4a and 4b)

An equimolar mixture of coumarin-based aldehyde (**1**) (1 mmol) and appropriate nitrile (**2a–2b**) (1 mmol) in EtOAc was initially stirred for half an hour at room temperature in the presence of 2–3 drops of Et_3N as a catalyst, and then 7-methyl-4-hydroxy coumarin (**3**) (1 mmol) was added. The course of the reaction was monitored by TLC. After completion of the reaction, the precipitates were formed, which were filtered and washed twice with hot ethyl acetate. Further purification was done by recrystallization using a mixture of $CHCl_3$ (4 parts) and MeOH (1 part) to furnish pure, newly synthesized heterocyclic coumarin-based pyrano-chromene compounds (**4a** and **4b**) with excellent yield. Physical and spectroscopic data for compounds (**4a** and **4b**) are shown below, while NMR and FT-IR spectra are shown in Fig. S1–S6.†

2.2 2-Amino-8-methyl-5-oxo-4-[2-(2-oxo-2*H*-chromen-3-ylmethoxy)-phenyl]-4*H*,5*H*-pyrano[3,2-*c*]chromene-3-carbonitrile (4a)

Colorless crystalline solid; m.p. 268–270 °C; yield: 97%; solubility: DMSO; FT-IR; KBr (cm^{-1}); 1681, 1718 (>C=O), 2180 (–CN), 3311, 3387 (NH_2-str.); ^{1}H NMR; (400 MHz, DMSO-d_6, δ, ppm) 2.37 (s, 3H, CH_3–H), 4.67 (s, 1H, CH, C_4–H), 4.80 (d, 1H, J = 10.2 Hz, OCH_2–H_a), 4.94 (d, 1H, J = 10.2 Hz, OCH_2–H_b), 6.89 (d, 1H, J = 6.4 Hz, Ar–H), 6.93 (t, 1H, J = 5.8 Hz, Ar–H), 7.07 (d, 1H, J = 6.5 Hz, Ar–H), 7.18–7.26 (m, 5H, NH_2–H, Ar–H), 7.34–7.37 (m, 3H, Ar–H), 7.51 (d, 1H, J = 6.2 Hz, Ar–H), 7.62 (td, 1H, J = 1.2 Hz, 7.3 Hz, Ar–H), 7.90 (s, 1H, CH, C_4'' – H); ^{13}C NMR; (100 MHz, DMSO-d_6, δ, ppm) 21.71, 33.98, 49.06, 57.12, 65.32, 102.68, 110.69, 113.03, 116.60, 116.79, 119.07, 120.11, 121.42, 121.95, 123.98, 124.94, 125.77, 128.90, 129.07, 131.06, 132.27, 141.43, 143.85, 152.47, 153.46, 154.40, 156.44, 158.80, 159.90, 160.33; anal. calcd. for $C_{30}H_{20}O_6N_2$ (504): C = 71.42, H = 4.00, N = 5.55; found (%): C = 71.35, H = 4.03, N = 5.58.

2.3 2-Amino-8-methyl-5-oxo-4-[2-(2-oxo-2*H*-chromen-3-ylmethoxy)-phenyl]-4*H*,5*H*-pyrano[3,2-*c*]chromene-3-carboxylic acid methyl ester (4b)

Colorless crystalline solid; m.p. 230–232 °C; yield: 92%; solubility (DMSO, $CHCl_3$); FT-IR; KBr (cm^{-1}); 1687, 1717 (>C=O), 3324, 3420 (NH_2-str.); ^{1}H NMR; (300 MHz, DMSO-d_6, δ, ppm) 2.13 (s, 3H, CH_3–H), 3.52 (s, 3H, COOMe–CH_3–H), 4.73 (d, 1H, J = 12.6 Hz, OCH_2–H_a), 4.76 (s, 1H, CH, C_4–H), 4.82 (d, 1H, J = 12.8 Hz, OCH_2–H_b), 6.90 (t, 1H, J = 7.2 Hz, Ar–H), 6.99 (d, 1H, J = 8.1 Hz, Ar–H), 7.16 (t, 1H, J = 7.5 Hz, Ar–H), 7.24–7.30 (m, 3H, Ar–H), 7.34–7.41 (m, 3H, Ar–H), 7.48 (d, 1H, J = 7.5 Hz, Ar–H), 7.62–7.67 (m, 3H, NH_2–H, Ar–H), 7.81 (s, 1H, CH, C_4'' – H); ^{13}C NMR, (75 MHz, DMSO-d_6, δ, ppm) 20.92, 34.02, 50.95, 65.50, 75.86, 105.11, 113.17, 113.29, 116.52, 116.64, 119.15, 120.78, 122.04, 124.17, 125.04, 128.43, 128.92, 131.81, 132.29, 132.59, 133.54, 134.02, 141.55, 150.60, 153.48, 153.90, 156.98, 159.36, 159.91, 160.52, 168.75; anal. calcd for $C_{31}H_{23}O_8N$ (537.14): C = 69.27, H = 4.31, N = 2.61; found (%): C = 69.24, H = 4.33, N = 2.68.

2.4 Chemistry

In order to obtain o-ring heterocyclic (pyrano-chromenes), a multicomponent approach was designed to synthesize novel fused ring coumarin-based dihydropyranochromenes (**4a** and **4b**) (Scheme 1). Coumarin-based aldehyde (**1**) was synthesized by utilizing the Baylis–Hillman reaction between salicylaldehyde and methyl acrylate.[47,48] The multi-component reaction of coumarin-based aromatic aldehyde (**1**), nitriles (**2a–2b**), and 7-methyl-4-hydroxy coumarin (**3**) in the presence of Et_3N through the Knoevenagel–Michael-cyclization path was utilized for the synthesis of these heterocyclic compounds with excellent yield. The optimization of various parameters like temperature, solvent, and catalyst, during the reaction was obtained to enhance the regioselectivity of the reaction as well as the yield of the product. Thus, ethyl acetate as solvent, Et_3N or Me_3N as a base, and 60 °C temperature were found to be the suitable parameters of choice for this reaction. The structures of synthesized compounds (**4a** and **4b**) were elaborated *via* spectroscopic techniques like FT-IR, NMR, and CHN analysis. In FTIR spectroscopic analysis, the C=O functional group appeared in the range of 1671–1718 cm^{-1}, while the cyano group appeared at 2179 cm^{-1}, and NH_2 groups in the relevant products were identified by absorption bands in the range of 3387–3420 cm^{-1}.

The ^1H NMR spectra of (**4a** and **4b**) gave evidence for cyclized products as there is no downfield signal of CHO proton at δ 10.48–10.53 ppm. Instead, a singlet of two protons for the NH_2 group was observed at δ 7.18–7.68 ppm and this peak is merged into the aromatic range by shielding or deshielding. Furthermore, the disappearance of the signal for the singlet of the OH group in 4-hydroxylated coumarins confirmed the cyclization. The appearance of one signal for the singlet of 3H at δ 3.34 ppm illustrated the presence of methyl-ester in compounds (**4b**). Total proton counts in the aromatic region also fulfill the structural requirements of the compound. Their chemical shifts were allocated on behalf of spin-multiplicity as well as coupling constant.

The ^{13}C NMR spectra of (**4a** and **4b**) unveiled the accordance of chemical shifts of aliphatic, aromatic, and carbonyl moieties with the desired structures. Further confirmation of the representative compounds (**4a** and **4b**) came from the absorption peaks of aliphatic carbons at 21.71, 33.98, and 49.06 ppm, aromatic carbons from 120 to 158 ppm, and carbonyl at 159.90 and 160.33 ppm. CHN analyses also favored the desired structures of pyrano-chromenes, as experimentally collected values were in accordance with calculated % ages. By utilizing the animation of Avogadro software, we calculated the results of vibrational analysis of fore-said compounds and compared with experimental results. The simulated stretching symmetrical and asymmetrical vibration band for $-NH_2$ groups in **4a** and **4b** are observed in the range of 3742–3509 and 3709–3538 cm^{-1}, respectively, which are in good harmony with experimental absorption bands (3466 and 3576 cm^{-1}, accordingly). Similarly, the experimentally determined stretching vibrational frequencies for –CN group in **4a** are found as 2361 cm^{-1} which showed good agreement with their DFT results (2376 cm^{-1}). The symmetrical stretching absorption bands for –CO are noted as 1886 and 1815 cm^{-1} while their experimental bands are determined at 1719 and 1716 cm^{-1}, respectively. Many other kind of simulated vibrations frequencies in **4a** and **4b** are also studied which showed good agreement with their experimental absorption bands (see in Tables S10, S11 and Fig. S5, S6†). In this research paper, the non-fullerene-natured synthesized crystals, *i.e.*, **4a** and **4b**, are evaluated in terms of their NLO characteristics. For this purpose, SC-XRD characterization is done and inspection of molecular configuration is carried out thoroughly *via* different parameters like bond lengths, bond angles, *etc.* The experimental data are compared with the theoretical results (DFT) to verify the chemical nature of the studied compounds.

2.5 Crystallization, data collection and structure solution

The crystals of compounds **4a** and **4b** were grown by slow evaporation in a methanol/chloroform solvent system in a 4 : 1. Colorless crystals appeared after a few days. Good quality single crystals were chosen for the diffraction experiment. The crystal was mounted on a goniometer head using grease. The data sets were collected on a Bruker D8 Venture with a PHOTON II detector and Mo microfocus source (λ = 0.71073 Å) (Bruker 2016) under ambient conditions using omega and phi scan methods. The diffracted intensities were processed using APEX3 tools. An analytical absorption correction was applied using the face indices of the crystal. Table 1 summarizes the crystallographic and refinement details.

Both the crystal structures were solved by direct methods in the triclinic ($P\bar{1}$) space group using Olex2 (ref. 49) (Fig. 1). All the

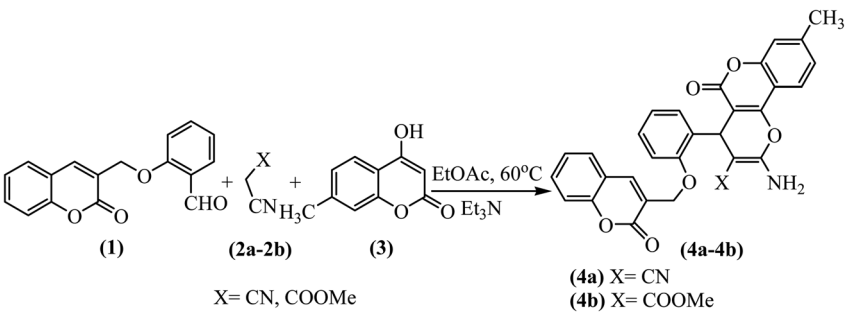

Scheme 1 Synthesis of coumarin-based pyrano-chromenes (**4a** and **4b**).

Table 1 Crystallographic data of compounds **4a** and **4b**

Comp.	**4a**	**4b**
Crystal data		
Chemical formula	$C_{30}H_{20}N_2O_6 \cdot CH_4O$	$C_{31}H_{23}NO_8$
M_r	536.55	537.50
Crystal system, space group	Triclinic, $P\bar{1}$	Triclinic, $P\bar{1}$
Temperature (K)	297(1)	297(1)
a, b, c (Å)	9.1201(7), 11.5487(7), 12.5810(8)	8.6139(15), 10.6283(16), 14.384(2)
α, β, γ (°)	93.498(2), 96.303(3), 100.317(3)	80.026(6), 80.436(7), 81.990(6)
V (Å^3)	1291.38(15)	1270.7(4)
Z	2	2
Radiation type	Mo Kα	Mo Kα
μ (mm^{-1})	0.10	0.10
Crystal size (mm)	0.22 × 0.18 × 0.17	0.32 × 0.22 × 0.13
Data collection		
Diffractometer	Bruker D8 Venture Photon II detector	
Absorption correction	Analytical SADABS2016/2 (Bruker, 2016/2) was used for absorption correction. wR_2(int) was 0.1247 before and 0.0684 after correction. The ratio of minimum to maximum transmission is 0.7828. The $\lambda/2$ correction factor is not present	
T_{min}, T_{max}	0.667, 0.746	0.584, 0.745
No. of measured, independent and observed [$I \geq 2u(I)$] reflections	35 003, 5884, 3085	33 043, 5205, 2618
R_{int}	0.064	0.083
(Sin $\theta/\lambda)_{max}$ (Å^{-1})	0.649	0.625
Refinement		
$R[F^2 > 2\sigma(F^2)]$, $wR(F^2)$, S	0.064, 0.248, 1.22	0.056, 0.194, 1.07
No. of reflections	5884	5205
No. of parameters	365	371
H-atom treatment	H-atom parameters constrained	H atoms are treated by a mixture of independent and constrained refinement
$\Delta\rangle_{max}$, $\Delta\rangle_{min}$ (e Å^{-3})	0.35, −0.35	0.29, −0.25

hydrogen atoms could be located in different Fourier maps. However, they are fixed using a riding model.

Both molecules crystallized with the $P\bar{1}$ space group. The asymmetric unit of **4a** contains one molecule of the organic compound along-with one molecule of methanol as solvent while the asymmetric unit of **4b** contains only one molecule of the organic moiety Fig. 1. The angles between the planes of the fitted atoms of pyrano-chromene ring system (C17–C29/O4/O6) and the central phenyl ring (C11–C16) are 88° and 88.35° in **4a** and **4b**, respectively, while the angles between the phenyl (C11–C16) and the coumarin ring system(C1–C9/O1) are 78.38° and 72.35° in **4a** and **4b**, respectively. The molecular structures (ORTEP diagrams) of coumarin-based pyrano-chromenes **4a** and **4b** with their crystallographic numbering are shown in Fig. 1.

In the case of **4a**, the molecular assembly is primarily built based on strong hydrogen bonds like N1–H1B···O2 and C14–H14···O5. Both interactions result in molecular dimerization. The interaction N1–H1B···O2, at a distance of 2.20(3) Å and N–H···O angle of 135.07(3)°, connects the molecules in dimers and generate twenty-four (24) membered ring motifs $R_2^2(24)$. Similarly, C14–H14···O5, connects the molecules to produce sixteen membered ring motifs $R_2^2(16)$, these two interactions go in a zigzag fashion at right angle. All these further extended into three-dimensional spaces through a large network of van der Waals's interactions. The amino group is involved in the formation of two hydrogen bonds. One we have discussed above while the other forms a hydrogen bond with N1–H1a···O7 at a distance of 2.171(3) Å and N–H···O angle of 155.1(3)° with the solvent molecule (methanol). The methanol molecule also forms another strong hydrogen bond with the reference molecule through the O7–H7A···O1 hydrogen bond (Fig. 2a). The hydroxyl group of methanol is bridging between the amino group and O1 of coumarin Fig. 2a. The interaction C3–H3···N2 connects the molecules along the diagonal of *ab*-plane. Other weak interactions from C5–H5···O5 and C3–H3···N2 generate fourteen membered ring motifs $R_3^2(14)$ Fig. 2a and Table 2.

Although the **4b** has no solvent of crystallization but it is affording three different type of hydrogen bonding interactions. There is one classical hydrogen bond between N1–H1b···O5 at a distance of 2.321(3) Å holding the successive molecules together in Fig. 2b. In addition, there is a nonclassical weak interaction from C13–H13···O2 interaction that help in the expansion of the molecular assembly along a-axis, base vector (1 0 0). There is an intramolecular hydrogen bonding interaction *via* N1–H1···O7 (Table 2) forming the stable six membered (H1A/N1/C20/C21/C22/O7) ring motif $S(6)$ with root mean square deviation of 0.0110(3) Å and this ring is fused with

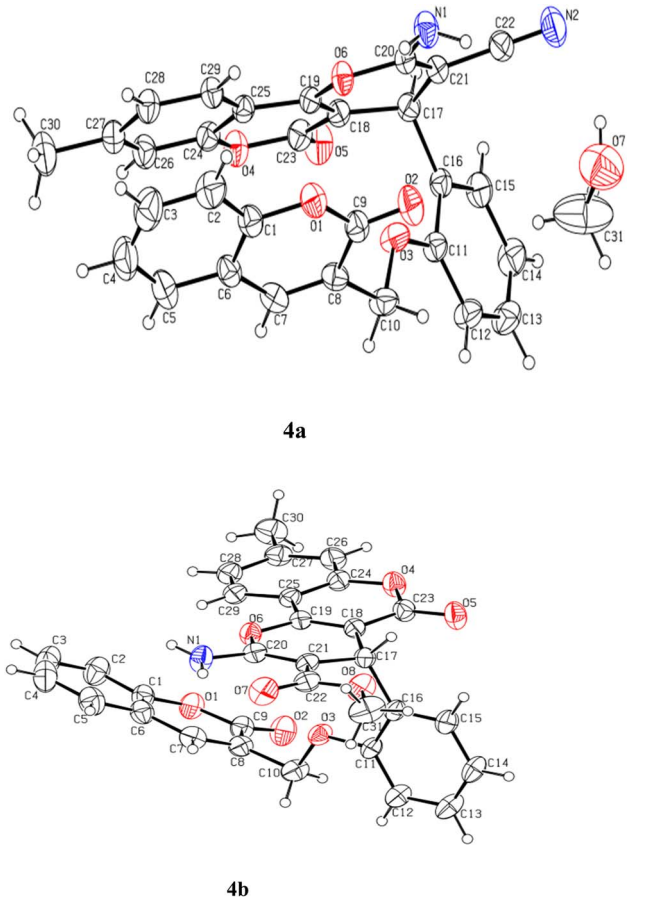

Fig. 1 View of the atom-labeled structures of compounds **4a** and **4b** (thermal ellipsoids were drawn at 30% probability level for both molecules).

another ring (O6/C20/C21/C17/C18/C19). The presence of more hydrogen bonds in **4a** than in **4b** lends higher thermal stability to the former, which is evident from the relatively higher m.p. of **4a** (268 °C) than in **4b** (230 °C). The root mean square deviation for the ring (O6/C20/C21/C17/C18/C19) is 0.0588(16) Å and puckering parameters are $Q = 0.144(3)$ Å, $\theta = 72.0(12)°$ and $\varphi = 176.9(11)°$ which are indicating that the ring is slightly deviating from planer to chair shape conformation. Both the rings (H1A/N1/C20/C21/C22/O7) and (O6/C20/C21/C17/C18/C19) are twisted by 4.232(4)°.

2.6 Hirshfeld surface and fingerprint plot analysis

Hirshfeld surface analysis allows us to quantify the various intermolecular interactions contributing to the packing of a whole molecule in a crystal.[50,51] The Hirshfeld surface and fingerprint plot of **4a** and **4b** molecules were mapped with d_{norm} (Fig. 3 and 4) using Crystal Explorer.[58] The white colour shows the contacts, which are close to Vander Waal's radii; the blue colour indicates the longer contacts; and the red colour represents the stronger interactions present in the crystal of HA. In Fig. 3, the surface map for **4a** represents the dark red region in the vicinity of O1, O2, and N1, showing the presence of strong O7–H7A···O1, N1–H1b···O2, and N1–H1a···O7, intermolecular interactions in the crystal. The rest of the surface does not show the presence of any strong interaction and appears neutral. These colour indications are very useful for the identification and relative strength of possible intermolecular interactions.

Similarly, in Fig. 4, the surface map for **4b** represents a single dark red region only in the vicinity of N1–H1b, while the rest of the surface appears neutral. These colour indications are very useful for the identification and relative strength of possible intermolecular interactions.

Fingerprint plots analyse the intermolecular interactions and molecular packing in a crystal on the basis of the Hirshfeld surface.[56–58] The fingerprint plots of **4a** and **4b** molecules are shown in Fig. 3 and 4. In both molecules, the H···H interactions predominate on the surface, with 39% and 40.2% contributions, respectively. This is followed by the contributions of O···H contacts, which account for 28.1% and 21.3%, respectively. Contributions by C···H interactions are next in the hierarchy, with values of 20.8% and 25.3%, respectively. The N···H contribution in **4a** is 11.6%, while in **4b** this contribution is very negligible (0.3%). The Hirshfeld surface map enables us to understand the intermolecular interactions and the strength of above-mentioned strong and weak interactions that contribute to the surface of the molecules.

2.7 Computational procedure

For the computational analysis of synthesized crystalline compounds **4a** and **4b**, the Gaussian 09 program package[52] was used. Primarily, the geometries of compounds were attained through SC-XRD by utilizing the crystallographic information file (CIF). Subsequently, DFT calculations for the entitled compounds were accomplished at M06-2X/6-31G(d,p) level of theory. Furthermore, NLO and FMOs analyses were performed for **4a** and **4b** at the aforementioned level of DFT, as well as NLO responses were calculated by using eqn (1)–(4).[53–55] However, natural bonding orbitals (NBOs) were investigated using the M06-2X/6-31G(d,p) level of theory,[56] because non-covalent interactions can be effectively studied at this level of theory. For interpretation of results from output files, Gauss View,[57] Avogadro,[58] Chemcraft,[59] PyMOlyze 2.0,[60] Origin 8.0,[61] and Multiwfn 3.7 (ref. 62) were employed.

$$\mu = (\mu_x^2 + \mu_y^2 + \mu_z^2)^{1/2} \quad (1)$$

$$\langle\alpha\rangle = (a_{xx} + a_{yy} + a_{zz})/3 \quad (2)$$

$$\beta_{tot} = (\beta_x^2 + \beta_y^2 + \beta_z^2)^{1/2} \quad (3)$$

where $\beta_x = \beta_{xxx} + \beta_{xyy} + \beta_{xzz}$, $\beta_y = \beta_{yxx} + \beta_{yyy} + \beta_{yzz}$ and $\beta_z = \beta_{zxx} + \beta_{zyy} + \beta_{zzz}$.

$$\gamma_{tot} = \sqrt{\gamma_x^2 + \gamma_y^2 + \gamma_z^2} \quad (4)$$

where $\gamma_i = \frac{1}{15}\sum_j(\gamma_{ijji} + \gamma_{ijij} + \gamma_{iijj}),\ i,\ j = \{x,\ y,\ z\}$

2.8 Result and discussions

In this research paper, the non-fullerene natured synthesized crystals, *i.e.*, **4a** and **4b** are evaluated in terms of their NLO

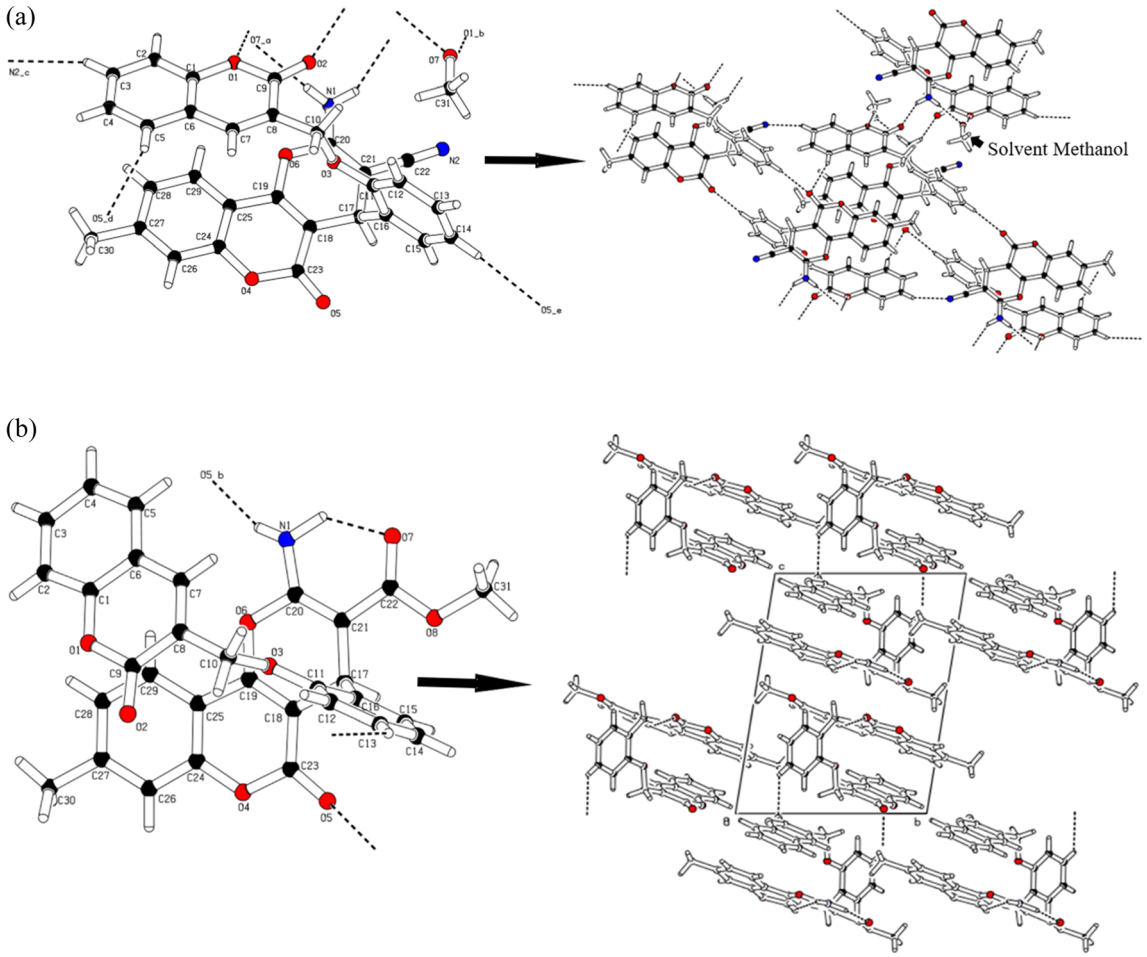

Fig. 2 (a) A diagram showing the hydrogen bonding interactions. Formation of dimer in through a centrosymmetric network of reciprocal strong N–H···O and bridging *via* O–H···O hydrogen bonds of methanol. (b) A diagram showing the hydrogen bonding interactions. Chain formation running along *a*-axis.

Table 2 Hydrogen bonds for **4a** and **4b**

D	H	A	*d*(D–H)/Å	*d*(H–A)/Å	*d*(D–A)/Å	D–H–A/°
4a						
N1	H1A	O7	0.86	2.17	2.973(4)	154.6
O7	H7A	O1	0.82	2.40	2.997(4)	130.7
N1	H1B	O2^{a}	0.86	2.20	2.874(3)	135.4
C14	H14	O5^{b}	0.93	2.55	3.470(4)	168.8
C3	H3	N2^{c}	0.93	2.61	3.483(4)	156.3
C5	H5	O5^{d}	0.93	2.60	3.433(4)	150.0
4b						
N1	H1A	O7	1.05(4)	1.84(4)	2.674(4)	133(3)
N1	H1B	O5^{e}	0.84(3)	2.32(3)	3.114(4)	158(3)
C13	H13	O2^{f}	0.93	2.55	3.221(4)	129.6

^{a} 1 − *X*, 1 − *Y*, −*Z*. ^{b} 1 − *X*, 2 − *Y*, 1 − *Z*. ^{c} −1 + *X*, −1 + *Y*, +*Z*. ^{d} −*X*, 1 − *Y*, 1 − *Z*. ^{e} 1 + *X*, +*Y*, +*Z*. ^{f} −*X*, 1 − *Y*, 2 − *Z*.

characteristics. For this purpose, SC-XRD characterization is done and inspection of molecular configuration is carried out thoroughly *via* different parameters like bond lengths, bond angles *etc.* The experimental data are compared with the theoretical results (DFT) in order to verify the chemical nature of the analyzed compounds. Moreover, the structural and optimized representation of entitled compounds is shown in Fig. 5.

2.9 Geometrical parameters

The geometrical parameters of entitled compounds were optimized at the M06-2X/6-31G(d,p) level of theory, and their data is organized in ESI (Tables S1 and S2†). The results of SC-XRD and DFT are found in excellent agreement with a few variations.

The simulated C–C bond lengths in the benzene ring of compound **4a** are found to be in the range of 1.162–1.507 Å, while in the range of 1.149–1.523 Å, as determined by XRD as shown in Table S1.† The bond lengths between carbon and oxygen atoms calculated through DFT are found to be 1.355, 1.366, 1.368, 1.364, 1.369, 1.415, 1.36, 1.385, 1.202, and 1.211 Å for O1–C10, O1–C15, O3–C20, O3–C22, O4–C9, O4–C31, O5–C17, O5–C18, O6–C18, and O7–C20, respectively, while through XRD the values were 1.366, 1.368, 1.373,1.375, 1.372, 1.431, 1.381, 1.387, 1.202, and 1.204 Å, respectively. Furthermore, the bond length for N2–C15 obtained by XRD is 1.342 Å, while the

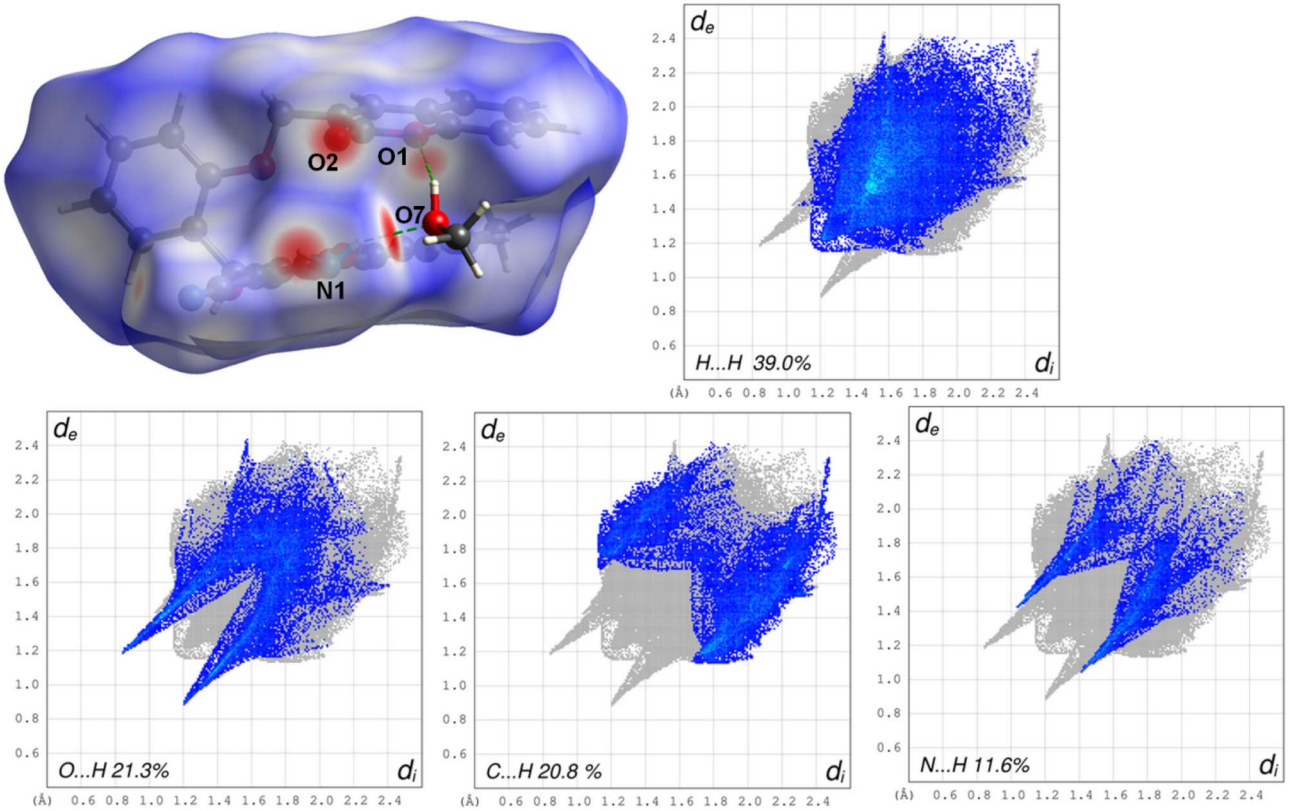

Fig. 3 A Hirshfeld surface of the **4a** showing the regions of strong interactions along with fingerprint plots showing the contributions of various interactions.

DFT calculated value for the above-mentioned bond length is examined to be 1.344 Å as given in Table S1.†

Similarly, for compound **4b**, the aforesaid bond lengths are observed in the range of 1.345–1.526 Å, which have good agreement with experimental data as 1.336–1.534 Å (see Table S2†). Moreover, for O1–C10, O1–C32, O2–C15, O2–C16, O3–C19, O3–C27, O4–C22, O4–C24, O5–C26, O5–C40, O6–C24, O7–C19, and O8–C26 bond lengths in compound **4b**, DFT values are noted to be 1.381, 1.418, 1.361, 1.364, 1.374, 1.362, 1.361, 1.38, 1.345, 1.425, 1.202, 1.205 and 1.224 Å, which are correspondingly matched with SC-XRD data at 1.381, 1.421, 1.364, 1.377, 1.376, 1.378, 1.376, 1.387, 1.338, 1.436, 1.215, 1.202, and 1.222 Å, respectively. For N9–C16 the bond length by both XRD and DFT calculation is found to be 1.355 Å and 1.336 Å, respectively.

In **4a**, bond angle values in C10–O1–C15, O1–C15–N2, N2–C15–C14, C20–O3–C22, O3–C20–C26, C9–O4–C31, O4–C9–C8, O4–C31–C26, C17–O5–C18, O5–C17–C27, O5–C18–C11, and O7–C20–C26 were observed through DFT as 118.3°, 110.4°, 117.6°, 122.8°,117.6°, 117.2°, 116°, 108.8°, 122.6°, 117.6°, 117.2°, and 124.8°, respectively. Similarly, through XRD, prominent values are 118.5°, 109.8°, 128°, 122.6°,117.8°, 118.3°, 115°, 106.2°, 121.9°, 117.7°, 118.1°, and 125.9°, respectively, as shown in Table S1.†

Similarly, in **4b**, the calculated bond angles between C10–O1–C32, O1–C10–C30, O1–C10–C35, O1–C32–C18, C15–O2–C16, O2–C15–C11, O2–C16–N9, O2–C16–C13, C19–O3–C27, O3–C19–O7, O3–C19–C18, O4–C22–C14, C26–O5–C40, O5–C26–O8, and N9–C16–C13 are observed through DFT as 114.7°, 120°, 118.9°, 107.9°,118.8°, 123.2°, 109.6°, 123°, 122.3°, 118.4°, 117°,114.7°, 121.6°, 115.1°, 121.6°, and 127.5 as well as 118.6°, 123.3°, 115.6°, 107.1°, 118.7°, 123.6°, 109.4°, 122.1°, 122.1°, 116.5°, 117.7°,114.7°, 121.2°, 117.6°, 121.7°, and 128.5° through XRD, respectively as shown in Table S2.† The torsion angles experimentally determined in the solid state are shown in Table S3.† The above-discussion explored that a good agreement is noted in computed and experimental findings, which confirms that M06-2X/6-31G(d,p) is suitable level of theory for DFT study. The geometrical structures are shown in Fig. S7.†

2.10 Frontier molecular orbitals (FMOs) analysis

The electronic characteristics of the studied molecules are investigated using the energies of HOMO/LUMO and their frontier molecular orbitals (FMOs) diagrams to calculate their chemical reactivity and stability.[63] The Lewis donor is commonly known HOMO (highest occupied molecular orbital) and the Lewis acceptor is called as LUMO (lowest unoccupied molecular orbital).[64,65] The electrons are transferred from the donor to the acceptor (HOMO to LUMO), which provides information about the intramolecular charge transfer (ICT) and NLO behavior.[66] An inverse relationship exists between the ΔE and ICT of a compound. Molecules with a greater ability to transfer charge between orbitals exhibit significant NLO properties with a lower ΔE value, and *vice versa*.[67] Herein, we

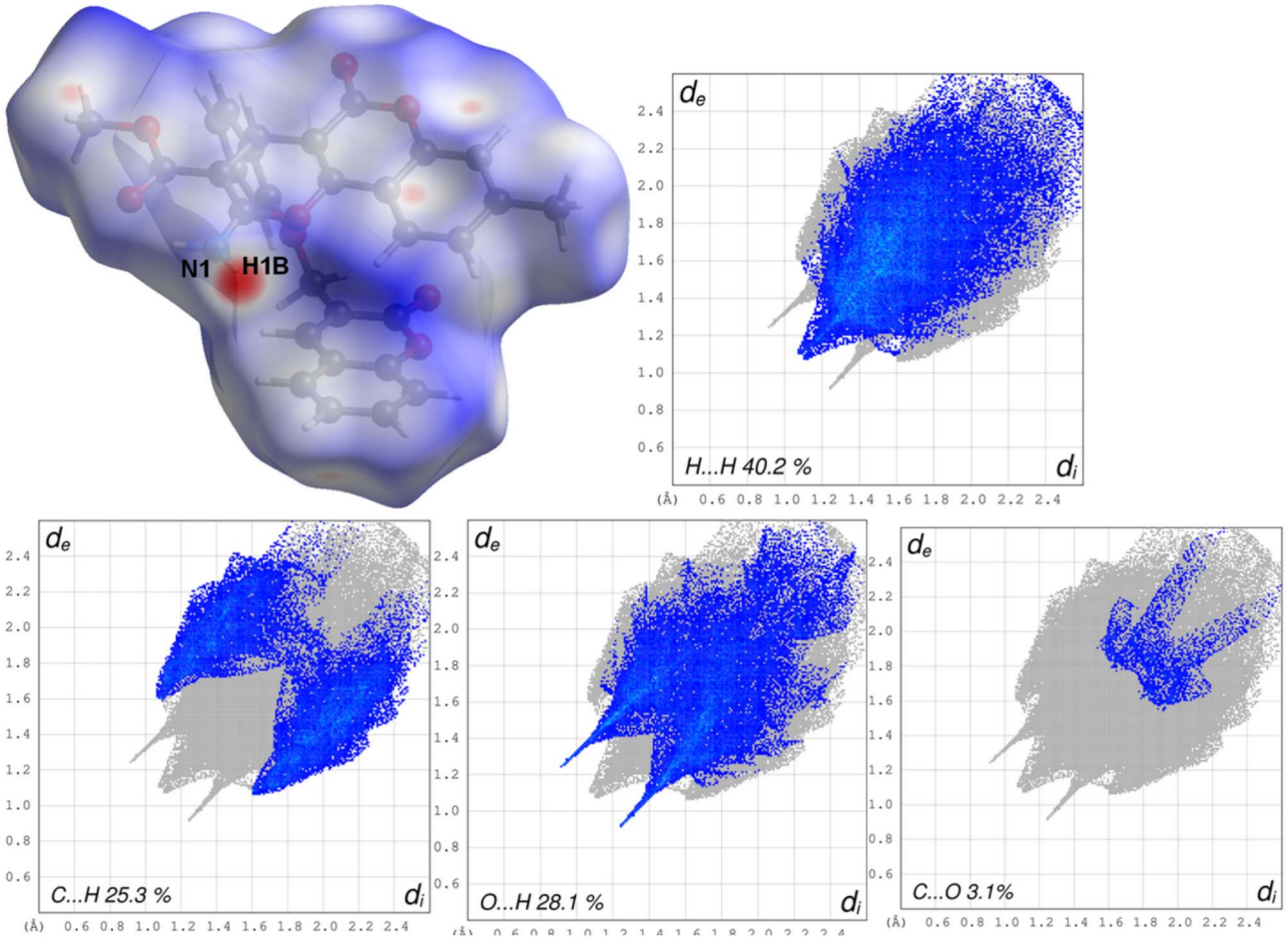

Fig. 4 A Hirshfeld surface of the **4b** showing the regions of strong interactions along with fingerprint plots showing the contributions of various interactions.

calculated the orbital energies and band gaps of our entitled compounds as shown in Table 3.

The data of energies obtained for **4a** are found to be −6.708 eV for HOMO and −1.540 eV for LUMO, while those for **4b** are noted to be −7.240 eV and −0.932 eV, respectively. The ΔE of **4a** is examined to be 5.168 eV, which is abridged to 6.308 eV in **4b**. Interestingly, a significant reduction in orbital energies and E_{gap} is observed for **4a** as compared to **4b**. This reduction of energies in **4a** is due to the presence of the nitro (–NO_2) group, as it is known that the nitro group has a stronger electron-withdrawing effect and inductive effect than the –CN group.[64] In addition to the energies of orbitals, ICT has also

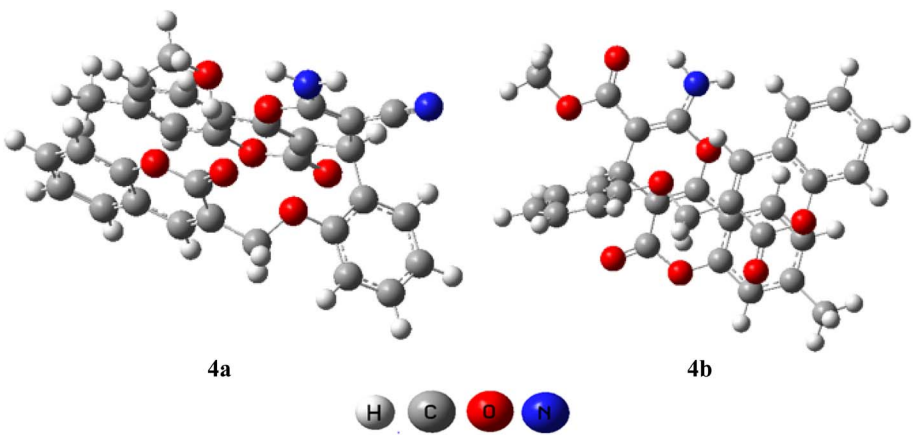

Fig. 5 The optimized structures of **4a** and **4b**.

Table 3 The energies of HOMO, LUMO and their energy gap for **4a** and **4b**

	4a		**4b**	
MOs	E (eV)	ΔE (eV)	E (eV)	ΔE (eV)
LUMO	−1.540	5.168	−0.932	6.308
HOMO	−6.708		−7.240	
LUMO+1	−0.700	6.669	−0.693	6.767
HOMO−1	−7.369		−7.460	
LUMO+2	−0.055	7.445	−0.436	7.330
HOMO−2	−7.500		−7.766	

been studied in the entitled compounds, as shown in Fig. S9.† The electronic charge density for HOMO is concentrated over the entire molecule in both compounds, while for LUMO the electronic cloud is distributed significantly all over the molecular region except the nitro and cyano groups in **4a** and **4b**, respectively.

2.11 Global reactivity descriptors

The stability and reactivity of **4a** and **4b** molecules can be excellently elaborated with various global reactivity parameters (GRPs) calculated by utilizing the LUMO–HOMO energy gap.[68] The results of these parameters, including electron affinity (EA), ionization potential (I),[69] global hardness (η),[70] global electrophilicity (ω),[71] electronegativity (X),[72] chemical potential (μ)[73] and global softness (σ), are estimated with the help of eqn (S5)–(S11)† and their outcomes are tabulated in Table S4.†

Ionization potential (IP) is the tendency to donate electrons, and electronegativity represents the ability to attract electrons.[68] Table 3 reveals that compound **4a** showed a higher value of electron affinity, electronegativity, and electrophilicity than compound **4b**. The reason for this enhanced value for **4a** might be the presence of highly electron-withdrawing nitro groups in the **4a** molecule. The parameters like chemical potential (μ) and hardness (η) are directly correlated with the energy gap. The compounds with the higher values of these parameters are considered as kinetically more stable and less reactive.[74] In our synthesized compounds, **4a** had a lower global hardness (η = 0.094 eV) and chemical potential (μ = −0.151 eV) with a higher softness (σ = 5.266 eV) than **4b**, indicating that **4a** is more kinetically stable and less reactive than **4b**. This GRPs investigation indicated that our prepared compounds are kinetically more stable and show excellent concurrence with NBO and SC-XRD data (Table 4).

2.12 Natural bond orbitals (NBOs) analysis

The NBOs are important for the investigation of bond interactions, the distribution of charges, and their delocalization among filled and vacant orbitals in a compound.[73] Moreover, the NBO analysis also facilitates the study of charge densities among various parts of a donor–π–acceptor molecule. It has been explored from the literature that most commonly the donor moiety holds a positive charge, while the acceptors are found with negatively charged values. Whereas, the π-spacer

Table 4 Ionization potential (IP), electron affinity (EA), electronegativity (X), chemical potential (μ), global hardness (η), global softness (σ) and global electrophilicity (ω)[a]

GRPs	**4a**	**4b**
IP	0.246	0.266
EA	0.056	0.034
X	0.151	0.150
η	0.094	0.116
μ	−0.151	−0.150
ω	0.121	0.097
σ	5.266	4.314

[a] Units are in eV.

may have positive or negative charges due to its role as a facilitator in the studied donor–π–acceptor framework. Assuming the above facts, the second-order perturbation theory of the said molecules is accomplished, and the stabilization energy for these molecules is calculated using eqn (5), which is as follows:

$$E^{(2)} = q_i \frac{(F_{i,j})^2}{\varepsilon_j - \varepsilon_i} \quad (5)$$

where, $E^{(2)}$ is the stabilization energy, ε_i and ε_j are off-diagonal, respectively; q_i is the donor orbital occupancy and $F_{i,j}$ is the diagonal NBO Fock matrix element. NBOs investigation is performed for entitled compounds, as elaborated in Table 5. However, some significant results are given in Tables S5 and S6.†

Four different forms of electronic transitions are frequently observed: π → π*, σ → σ*, LP → π*, and LP → σ*. The most dominant electronic transitions are found as π → π* among the above-mentioned transitions, while σ → σ* is examined as the least prominent, and LP → π* and LP → σ* are noticed as slightly dominant transitions.

In the case of compound **4a**, the most prominent π → π* transitions are π(C27–C33) → π*(C12–C17) and π(C8–C24) → π*(C14–C15), which showed the highest and the least energies of stabilization as 34.85 and 0.56 kcal mol^{-1}, respectively. The weaker σ → σ* transitions are also examined with some prominent values as 6.80 and 0.51 kcal mol^{-1} observed in transitions σ(C11–C18) → σ*(O1–C10) and σ(C26–C31) → σ*(C31–H54), respectively. Some resonance transitions that are also important for discussion include LP1(N2) → π*(C14–C15), which determined the highest stabilization energy of 77.62 kcal mol^{-1}, and LP1(O8) → σ*(C31–H55), which showed the lowest stabilization energy of 0.66 kcal mol^{-1} (see Table 5).

In compound **4b**, the highest stabilization energy obtained is 34.95 kcal mol^{-1}, which is exhibited during π(C16–C19) → π*(O8–C33) transitions, while, π(O7–C23) → π*(O7–C23) is noted with the smallest stabilization energy value as 0.78 kcal mol^{-1}. The other feeble electronic transitions that are significant to discuss for compound **4a** are: σ(C13–C30) → σ*(O2–C18), σ(C22–C28) → σ*(C42–H43), LP2(O5) → π*(O8–C33), and LP1(O8) → σ*(O5–C60), which showed energies of 6.82, 0.51, 59.26, and 0.50 kcal mol^{-1}, respectively.

Overall, the results obtained from the above discussion validate the formation of charge separation states in the

Table 5 Fock matrix investigation for the studied compounds (**4a** and **4b**)

Comp.	Donor (i)	Type	Acceptor (j)	Type	$E^{(2)a}$ [kcal mol^{-1}]	$E(j) - E(i)^b$ (a.u.)	$F(i,j)^c$ (a.u.)
4a	C27–C33	π	C12–C17	π*	34.85	0.34	0.100
	C8–C24	π	C14–C15	π*	0.56	0.34	0.013
	C11–C18	σ	O1–C10	σ*	6.80	1.20	0.081
	C26–C31	σ	C31–H54	σ*	0.51	1.23	0.022
	N2	LP(1)	C14–C15	π*	77.62	0.36	0.153
	O4	LP(1)	C31–H55	σ*	0.66	1.15	0.025
4b	C16–C19	π	O8–C33	π*	34.95	0.37	0.106
	O7–C23	π	O7–C23	π*	0.78	0.51	0.019
	C13–C30	σ	O2–C18	σ*	6.82	1.19	0.080
	C22–C28	σ	C42–H43	σ*	0.51	1.34	0.023
	O5	LP(2)	O8–C33	π*	59.26	0.43	0.148
	O8	LP(1)	O5–C60	σ*	0.50	1.14	0.021

[a] $E^{(2)}$ represents the energy of hyper conjugative interaction (stabilization energy in kcal mol^{-1}). [b] Energy difference between D and A NBO orbitals. [c] $F(i,j)$ is the Fock matrix element between i and j NBO orbitals.

investigated molecules. Whereas, the stabilization energies also revealed comparable stability in both compounds, for which the ICT, conjugation, and hyper conjugative interactions might be the main reasons for their stabilities.

2.13 UV-vis analysis

The UV-Vis absorption spectra of the coumarin-based pyranochromene derivatives **4a** and **4b** in chloroform, dimethyl sulfoxide (DMSO), and 1,4-dioxane were recorded at room temperature. TDDFT UV-Vis absorption data were calculated in the gas phase. This study provides a reasonable apprehension of optoelectronic properties, probability of charge transfer, and molecular orbital configurations of electronic transitions for the studied compounds.[75–77] The TD-DFT methodology was employed using the above-mentioned level of theory to execute the UV-Vis absorption spectra. Table 6 presents the data obtained for **4a** and **4b**, including the maximum wavelength (λ_{max}), vertical excitation energies (eV), oscillator strength (f_{os}), and orbital transitions. The detailed results are recorded in Table S7,† and graphs of absorption maxima for both compounds are displayed in Fig. S8.†

The data obtained from the analysis show the λ_{max} of **4a** and **4b** are 268.579 and 269.513 nm, respectively. Interestingly, the experimentally calculated values (in solvents *i.e.*, chloroform, 1,4-dioxane, and DMSO) of λ_{max} are found bathochromically shifted as compared to the theoretical values (in the gas phase) of compounds (**4a** and **4b**), which may occur due to change in environmental conditions as expressed in Table 6. **4a** displayed a value of the absorbance at 268.579 nm with corresponding oscillation strength of 0.337 and 4.616 eV transition energy, which are associated with H−1 → L (68%) as a major contribution. Similarly, λ_{max} calculated in the case of **4b** was 269.513 nm with two major transitions as H → L+1 (36%), and H−1 → L+2 (30%), possessing oscillation strengths of 0.374 and 4.600 eV transition energy.

2.14 Non-linear optical (NLO) properties

Non-linear optical materials have immense potential in photonics with striking applications in the optoelectronics and telecommunication sectors.[74,75] The NLO response varies with the variation of the position of diverse substituents on the compounds. Here, we compute the statistical average of molecular dipoles moment (u), linear and non-linear responses of **4a** and **4b** at the aforementioned level of theory, and the major results are tabulated in Table 7, whereas the detailed calculations are present in the ESI (Tables S8 and S9†).

Table S8† holds the linear polarizability with major contributing tensors along the x, y, and z-axes. The polarizability tensor along the x-direction (α_{xx}) shows the highest value and thus has more contribution towards linear polarizability in

Table 6 Computed transition energy (eV), maximum absorption wavelengths (λ_{max}), oscillator strengths (f_{os}), and transition natures of title compounds

Comp.	Exp. λ_{max} (nm)	DFT λ_{max} (nm)	E (eV)	f_{os}	MO contributions
4a	— 335.5[a] 328.5[b] 337.5[c]	268.579[d]	4.616	0.337	H−1 → L (68%), H → L (2%)
4b	— 339[a] 331.5[b] 317[c]	269.513[d]	4.600	0.374	H → L+1 (36%), H−1 → L+2 (30%)

[a] Chloroform. [b] 1,4-Dioxane. [c] DMSO. [d] Gas phase.

Table 7 The statistical average of molecular dipoles, linear polarizability, and hyperpolarizabilities for compounds (**4a** and **4b**)

Comp.	μ_{tot}	$\langle\alpha\rangle \times 10^{-23}$	$\gamma_{tot} \times 10^4$
4a	6.236	6.770	0.145
4b	3.256	6.699	0.145

both **4a** and **4b** compounds. The total values of statistical average of molecular dipoles moment (μ_{tot}), average polarizability $\langle\alpha\rangle$, and second order hyperpolarizability (γ_{tot}) are also shown in Table 7. The μ_{tot} is found to be 6.236 and 3.256 D, for compounds **4a** and **4b**, respectively. The highest computed value of statistical average of molecular dipoles moment exists for compound **4a** as 6.236 D, while the smallest amplitude of 3.256 D is examined for compound **4b**. All the entitled molecules showed significant statistical average of molecular dipoles moment values when compared with the standard urea molecule, which showed a value of 1.3732 D (ref. 78) (Table S8†). The average linear polarizability $\langle\alpha\rangle$ values for compounds **4a** and **4b** are observed to be 6.770×10^{-23} and 6.699×10^{-23} esu, respectively. Hence, the greater $\langle\alpha\rangle$ value is noticed in **4a** as compared to **4b**.

The second-order polarizability (γ_{tot}) values are observed in both the studied compounds as 0.145×10^4 esu. It is also observed that the highest contributing value of γ_{tot} for **4a** is shown along the *z*-axis ($\gamma_{zz} = 2.324 \times 10^4$ esu) and for **4b** along the *x*-axis (8.907×10^4 esu), which indicates the higher polarization along the *z* and *x*-directions for titled compounds (Table S8†). Interestingly, in our studied crystals, remarkable NLO results were obtained as their various parameters such as μ_{tot}, $\langle\alpha\rangle$, and γ_{tot} when compared with urea molecule.[79,80] This comparative analysis of **4a** and **4b** with urea found to be many folds higher than urea. This urea-related examination implied that all considered molecules were appropriate to be NLO entities. This showed their effective structural tailoring using efficient donor and acceptor moieties to obtain significant NLO materials. The orientation of the **4a** and **4b** molecule along *x*, *y* and *z* axis are shown in Fig. S10 and S11.†

3. Conclusion

The current work indicates the quantum chemical investigation of two novel coumarin-based pyrano-chromene crystal chromophores, **4a** and **4b**. The compounds were synthesized in a good yield through the Knoevenagel–Michael-cyclization path using a one-pot multicomponent reaction. The structures of these o-ring heterocyclic compounds were ascertained by spectroscopic techniques like UV-Vis, FT-IR, ^{1}H & ^{13}C NMR, and single crystal X-ray diffraction analysis. The SC-XRD analysis of **4a** and **4b** revealed the triclinic crystal lattice with space group $P\bar{1}$. The spectroscopic results were found to be in good agreement with the SC-XRD data. The DFT and SC-XRD data were also perceived in good accordance, as shown by their computed bond lengths and bond angles. The NBO probe also confirmed the presence of charge separation, which showed that the entitled compounds are involved in the process of ICT, hence, endorsing their higher molecular stability. The higher energy band gap of **4b** (6.308 eV) as compared to **4a** (5.168 eV) was obtained due to the presence of highly electronegative cyano group in **4b**. The GRPs were derived utilizing energies of HOMOs and LUMOs of said compounds. Fantastically, large $\langle\alpha\rangle$ and γ_{tot} responses are computed for **4a** than that of standard urea molecule. We infer that the present DFT-based study might be regarded as a remarkable achievement and may have prospective applications in developing new NLO materials.

Conflicts of interest

There are no conflicts to declare.

Acknowledgements

The authors would like to thank King Khalid University's Deanship of Scientific Research for funding this study under grant number (R.G.P.1/28/43). Dr Muhammad Khalid gratefully acknowledges the financial support of HEC Pakistan (project no. 20-14703/NRPU/R&D/HEC/2021). Authors are also thankful for cooperation and collaboration of A. A. C. B. from IQ-USP, Brazil especially for his continuous support and providing computational lab facilities.

References

1 J. D. Sunderhaus and S. F. Martin, Applications of multicomponent reactions to the synthesis of diverse heterocyclic scaffolds, *Chem.–Eur. J.*, 2009, **15**, 1300–1308.
2 K. C. Nicolaou, J. A. Pfefferkorn, H. J. Mitchell, A. J. Roecker, S. Barluenga, G.-Q. Cao, R. L. Affleck and J. E. Lillig, Natural product-like combinatorial libraries based on privileged structures. 2. Construction of a 10 000-membered benzopyran library by directed split-and-pool chemistry using NanoKans and optical encoding, *J. Am. Chem. Soc.*, 2000, **122**, 9954–9967.
3 K. C. Nicolaou, J. A. Pfefferkorn, S. Barluenga, H. J. Mitchell, A. J. Roecker and G.-Q. Cao, Natural product-like combinatorial libraries based on privileged structures. 3. The "libraries from libraries" principle for diversity enhancement of benzopyran libraries, *J. Am. Chem. Soc.*, 2000, **122**, 9968–9976.
4 G. M. Cragg and D. J. Newman, Natural products: a continuing source of novel drug leads, *Biochim. Biophys. Acta, Gen. Subj.*, 2013, **1830**, 3670–3695.
5 A. Jashari, F. Imeri, L. Ballazhi, A. Shabani, B. Mikhova, G. Dräger, E. Popovski and A. Huwiler, Synthesis and cellular characterization of novel isoxazolo-and thiazolohydrazinylidene-chroman-2,4-diones on cancer and non-cancer cell growth and death, *Bioorg. Med. Chem.*, 2014, **22**, 2655–2661.
6 X.-M. Peng, G. L. V. Damu and H. Zhou, Current developments of coumarin compounds in medicinal chemistry, *Curr. Pharm. Des.*, 2013, **19**, 3884–3930.
7 L. Ma, Y. Xiao, C. Li, Z.-L. Xie, D.-D. Li, Y.-T. Wang, H.-T. Ma, H.-L. Zhu, M.-H. Wang and Y.-H. Ye, Synthesis and

antioxidant activity of novel Mannich base of 1,3,4-oxadiazole derivatives possessing 1,4-benzodioxan, *Bioorg. Med. Chem.*, 2013, **21**, 6763–6770.

8 M. A. Musa, V. L. Badisa, L. M. Latinwo, J. Cooperwood, A. Sinclair and A. Abdullah, Cytotoxic activity of new acetoxycoumarin derivatives in cancer cell lines, *Anticancer Res.*, 2011, **31**, 2017–2022.

9 P. Borah, P. S. Naidu and P. J. Bhuyan, Synthesis of some tetrazole fused pyrido[2,3-c]coumarin derivatives from a one-pot three-component reaction via intramolecular 1,3-dipolar cycloaddition reaction of azide to nitriles, *Tetrahedron Lett.*, 2012, **53**, 5034–5037.

10 M. Ninomiya, K. Shirabe, H. Kayashima, T. Ikegami, A. Nishie, N. Harimoto, Y. Yamashita, T. Yoshizumi, H. Uchiyama and Y. Maehara, Functional assessment of the liver with gadolinium–ethoxybenzyl-diethylenetriamine penta-acetate-enhanced MRI in living-donor liver transplantation, *Br. J. Surg.*, 2015, **102**, 944–951.

11 G. J. Keating, J. G. Quinn and R. O'Kennedy, *Immunoassay for the determination of 7-hydroxycoumarin in serum using 'real-time' biosensor analysis*, 1999.

12 J. Neyts, E. D. Clercq, R. Singha, Y. H. Chang, A. R. Das, S. K. Chakraborty, S. C. Hong, S.-C. Tsay, M.-H. Hsu and J. R. Hwu, Structure-activity relationship of new anti-Hepatitis C virus agents: heterobicycle-coumarin conjugates, *J. Med. Chem.*, 2009, **52**, 1486–1490.

13 U. Salar, K. M. Khan, A. Jabeen, S. Hussain, A. Faheem, F. Naqvi and S. Perveen, Diversified Thiazole Substituted Coumarins and Chromones as Non-Cytotoxic ROS and NO Inhibitors, *Lett. Drug Des. Discovery*, 2020, **17**, 547–555.

14 K. V. Sashidhara, A. Kumar, M. Kumar, J. Sarkar and S. Sinha, Synthesis and in vitro evaluation of novel coumarin–chalcone hybrids as potential anticancer agents, *Bioorg. Med. Chem. Lett.*, 2010, **20**, 7205–7211.

15 C. A. Kontogiorgis and D. J. Hadjipavlou-Litina, Synthesis and antiinflammatory activity of coumarin derivatives, *J. Med. Chem.*, 2005, **48**, 6400–6408.

16 R. S. Keri, B. S. Sasidhar, B. M. Nagaraja and M. A. Santos, Recent progress in the drug development of coumarin derivatives as potent antituberculosis agents, *Eur. J. Med. Chem.*, 2015, **100**, 257–269.

17 G. Borges Bubols, D. da Rocha Vianna, A. Medina-Remon, G. von Poser, R. M. Lamuela-Raventos, V. Lucia Eifler-Lima and S. Cristina Garcia, The antioxidant activity of coumarins and flavonoids, *Mini-Rev. Med. Chem.*, 2013, **13**, 318–334.

18 T. Matsumoto, K. Takahashi, S. Kanayama, Y. Nakano, H. Imai, M. Kibi, D. Imahori, T. Hasei and T. Watanabe, Structures of antimutagenic constituents in the peels of Citrus limon, *J. Nat. Med.*, 2017, **71**, 735–744.

19 O. M. Abdelhafez, K. M. Amin, R. Z. Batran, T. J. Maher, S. A. Nada and S. Sethumadhavan, Synthesis, anticoagulant and PIVKA-II induced by new 4-hydroxycoumarin derivatives, *Bioorg. Med. Chem.*, 2010, **18**, 3371–3378.

20 Y. K. Al-Majedy, A. A. Al-Amiery, A. A. H. Kadhum and A. B. Mohamad, Antioxidant activities of 4-methylumbelliferone derivatives, *PLoS One*, 2016, **11**, e0156625.

21 A. Nargotra, S. Sharma, M. I. Alam, Z. Ahmed, A. Bhagat, S. C. Taneja, G. N. Qazi and S. Koul, In silico identification of viper phospholipaseA2 inhibitors: validation by in vitro, in vivo studies, *J. Mol. Model.*, 2011, **17**, 3063–3073.

22 O. S. Kwon, J. S. Choi, M. Islam, Y. S. Kim and H. P. Kim, Inhibition of 5-lipoxygenase and skin inflammation by the aerial parts of Artemisia capillaris and its constituents, *Arch. Pharmacal Res.*, 2011, **34**, 1561–1569.

23 T. Thomas, Monoamine oxidase-B inhibitors in the treatment of Alzheimers disease, *Neurobiol. Aging*, 2000, **21**, 343–348.

24 P. O. Patil, S. B. Bari, S. D. Firke, P. K. Deshmukh, S. T. Donda and D. A. Patil, *Bioorg. Med. Chem.*, 2013, **21**, 2434–2450.

25 I. Kostova, Synthetic and natural coumarins as cytotoxic agents, *Curr. Med. Chem.: Anti-Cancer Agents*, 2005, **5**, 29–46.

26 K. Biradha, Crystal engineering: from weak hydrogen bonds to co-ordination bonds, *CrystEngComm*, 2003, **5**, 374–384.

27 R. Jawaria, M. Hussain, Z. Shafiq, H. B. Ahmad, M. N. Tahir, H. A. Shad and M. M. Naseer, Robustness of thioamide dimer synthon, carbon bonding and thioamide–thioamide stacking in ferrocene-based thiosemicarbazones, *CrystEngComm*, 2015, **17**(12), 2553–2561.

28 S. K. Seth, D. Sarkar and T. Kar, Use of π–π forces to steer the assembly of chromone derivatives into hydrogen bonded supramolecular layers: crystal structures and Hirshfeld surface analyses, *CrystEngComm*, 2011, **13**, 4528–4535.

29 M. Małecka, L. Chęcińska, A. Rybarczyk-Pirek, W. Morgenroth and C. Paulmann, Electron density studies on hydrogen bonding in two chromone derivatives, *Acta Crystallogr., Sect. B: Struct. Sci.*, 2010, **66**, 687–695.

30 A. Poursattar Marjani, B. Ebrahimi Saatluo and F. Nouri, An efficient synthesis of 4H-chromene derivatives by a one-pot, three-component reaction, Iran, *Iran. J. Chem. Chem. Eng.*, 2018, **37**, 149–157.

31 M. R. Khumalo, S. N. Maddila, S. Maddila and S. B. Jonnalagadda, A facile and one-pot synthesis of new tetrahydrobenzo[b]pyrans in water under microwave irradiation, *BMC Chem.*, 2019, **13**, 1–7.

32 D. Kumar, V. B. Reddy, S. Sharad, U. Dube and S. Kapur, A facile one-pot green synthesis and antibacterial activity of 2-amino-4H-pyrans and 2-amino-5-oxo-5,6,7,8-tetrahydro-4H-chromenes, *Eur. J. Med. Chem.*, 2009, **44**, 3805–3809.

33 A. M. El-Saghier, M. B. Naili, B. K. Rammash, N. A. Saleh and K. M. Kreddan, Synthesis and antibacterial activity of some new fused chromenes, *Arkivoc*, 2007, **16**, 83–91.

34 Ž. B. Milanović, Z. S. Marković, D. S. Dimić, O. R. Klisurić, I. D. Radojević, D. S. Šeklić, M. N. Živanović, J. D. Marković, M. Radulović and E. H. Avdović, Synthesis, structural characterization, biological activity and molecular docking study of 4,7-dihydroxycoumarin modified by aminophenol derivatives, *C. R. Chim.*, 2021, **24**, 215–232.

35 P. M. Ronad, M. N. Noolvi, S. Sapkal, S. Dharbhamulla and V. S. Maddi, Synthesis and antimicrobial activity of 7-(2-

substituted phenylthiazolidinyl)-benzopyran-2-one derivatives, *Eur. J. Med. Chem.*, 2010, **45**, 85–89.

36 R. Devakaram, D. S. Black, K. T. Andrews, G. M. Fisher, R. A. Davis and N. Kumar, Synthesis and antimalarial evaluation of novel benzopyrano[4,3-b]benzopyran derivatives, *Bioorg. Med. Chem.*, 2011, **19**, 5199–5206.

37 S. M. Hasan, M. M. Alam, A. Husain, S. Khanna, M. Akhtar and M. S. Zaman, Synthesis of 6-aminomethyl derivatives of benzopyran-4-one with dual biological properties: anti-inflammatory-analgesic and antimicrobial, *Eur. J. Med. Chem.*, 2009, **44**, 4896–4903.

38 A. E.-F. G. Hammam, Novel fluoro substituted benzo[*b*] pyran with anti-lung cancer activity, *Indian J. Chem., Sect. B: Org. Chem. Incl. Med. Chem.*, 2005, **44B**, 1887–1893.

39 I. P. Singh and H. S. Bodiwala, Recent advances in anti-HIV natural products, *Nat. Prod. Rep.*, 2010, **27**, 1781–1800.

40 M. Nawaz, M. W. Abbasi and S. Hisaindee, Synthesis, characterization, anti-bacterial, anti-fungal and nematicidal activities of 2-amino-3-cyanochromenes, *J. Photochem. Photobiol., B*, 2016, **164**, 160–163.

41 I. Fatima, R. Saxena, G. Kharkwal, M. K. Hussain, N. Yadav, K. Hajela, P. L. Sankhwar and A. Dwivedi, The anti-proliferative effect of 2-[piperidinoethoxyphenyl]-3-[4-hydroxyphenyl]-2H-benzo(b)pyran is potentiated via induction of estrogen receptor beta and p21 in human endometrial adenocarcinoma cells, *J. Steroid Biochem. Mol. Biol.*, 2013, **138**, 123–131.

42 C. Corminboeuf, F. Tran and J. Weber, The role of density functional theory in chemistry: some historical landmarks and applications to zeolites, *J. Mol. Struct.: THEOCHEM*, 2006, **762**, 1–7.

43 M. Ashfaq, A. Ali, A. Kuznetsov, M. N. Tahir and M. Khalid, DFT and single-crystal investigation of the pyrimethamine-based novel co-crystal salt: 2,4-diamino-5-(4-chlorophenyl)-6-ethylpyrimidin-1-ium-4-methylbenzoate hydrate (1:1:1) (DEMH), *J. Mol. Struct.*, 2021, **1228**, 129445, DOI: **10.1016/j.molstruc.2020.129445**.

44 E. H. Avdović, D. S. Dimić, M. Fronc, J. Kožišek, E. Klein, Ž. B. Milanović, A. Kesić and Z. S. Marković, Structural and theoretical analysis, molecular docking/dynamics investigation of 3-(1-m-chloridoethylidene)-chromane-2,4-dione: the role of chlorine atom, *J. Mol. Struct.*, 2021, **1231**, 129962.

45 A. Ali, M. Khalid, M. F. U. Rehman, S. Haq, A. Ali, M. N. Tahir, M. Ashfaq, F. Rasool and A. A. C. Braga, Efficient synthesis, SC-XRD, and theoretical studies of O-benzenesulfonylated pyrimidines: role of noncovalent interaction influence in their supramolecular network, *ACS Omega*, 2020, **5**, 15115–15128.

46 M. Akram, M. Adeel, M. Khalid, M. N. Tahir, M. U. Khan, M. A. Asghar, M. A. Ullah and M. Iqbal, A combined experimental and computational study of 3-bromo-5-(2,5-difluorophenyl)pyridine and 3,5-bis(naphthalen-1-yl) pyridine: insight into the synthesis, spectroscopic, single crystal XRD, electronic, nonlinear optical and biological properties, *J. Mol. Struct.*, 2018, **1160**, 129–141.

47 P. T. Kaye, M. A. Musa, X. W. Nocanda and R. S. Robinson, Does the DABCO-catalysed reaction of 2-hydroxybenzaldehydes with methyl acrylate follow a Baylis–Hillman pathway?, *Org. Biomol. Chem.*, 2003, **1**, 1133–1138.

48 A. Hameed, Z. Shafiq, M. Yaqub, M. Hussain, H. B. Ahmad, M. N. Tahir and M. M. Naseer, Robustness of a thioamide $\{\cdots H–N–C{=}S\}_2$ synthon: synthesis and the effect of substituents on the formation of layered to cage-like supramolecular networks in coumarin–thiosemicarbazone hybrids, *New J. Chem.*, 2015, **39**, 6052–6061.

49 O. V. Dolomanov, L. J. Bourhis, R. J. Gildea, J. A. K. Howard and H. Puschmann, *J. Appl. Crystallogr.*, 2009, **42**, 339–341.

50 D. Milenković, E. Avdović, D. Dimić, S. Sudha, D. Ramarajan, Ž. Milanović, S. Trifunović, Z. Marković and N. B. O. Vibrational, Hirshfeld surface analyses and molecular docking study of m-toluidine-coumarin derivative and its corresponding palladium(II) complex, *J. Mol. Struct.*, 2020, **1209**, 127935.

51 Ž. B. Milanović, D. S. Dimić, E. H. Avdović, D. A. Milenković, J. D. Marković, O. R. Klisurić, S. R. Trifunović and Z. S. Marković, Synthesis and comprehensive spectroscopic (X-ray, NMR, FTIR, UV-Vis), quantum chemical and molecular docking investigation of 3-acetyl-4-hydroxy-2-oxo-2H-chromen-7-yl acetate, *J. Mol. Struct.*, 2021, **1225**, 129256.

52 M. J. Frisch, G. W. Trucks, H. B. Schlegel, G. E. Scuseria, M. A. Robb, J. R. Cheeseman, G. Scalmani, V. Barone, B. Mennucci and G. A. Petersson, *Gaussian 09, Revision D.01*, Gaussian, Inc., Wallingford, CT, 2009.

53 A. Alparone, Linear and nonlinear optical properties of nucleic acid bases, *Chem. Phys.*, 2013, **410**, 90–98.

54 A. Plaquet, M. Guillaume, B. Champagne, F. Castet, L. Ducasse, J.-L. Pozzo and V. Rodriguez, In silico optimization of merocyanine-spiropyran compounds as second-order nonlinear optical molecular switches, *Phys. Chem. Chem. Phys.*, 2008, **10**, 6223–6232.

55 K. B. Lipkowitz and D. B. Boyd, *Reviews in Computational Chemistry*, John Wiley & Sons, 2009, vol. 12.

56 J.-D. Chai and M. Head-Gordon, Long-range corrected hybrid density functionals with damped atom–atom dispersion corrections, *Phys. Chem. Chem. Phys.*, 2008, **10**, 6615–6620.

57 R. D. Dennington, T. A. Keith and J. M. Millam, *GaussView 5.0*, Gaussian, Inc., Wallingford, 2008.

58 M. D. Hanwell, D. E. Curtis, D. C. Lonie, T. Vandermeersch, E. Zurek and G. R. Hutchison, Avogadro: an advanced semantic chemical editor, visualization, and analysis platform, *J. Cheminf.*, 2012, **4**, 1–17.

59 G. A. Zhurko and D. A. Zhurko, *ChemCraft, Version 1.6*, 2009, **https://www.chemcraftprog.com**.

60 N. M. O'boyle, A. L. Tenderholt and K. M. Langner, Cclib: a library for package-independent computational chemistry algorithms, *J. Comput. Chem.*, 2008, **29**, 839–845.

61 L. A. Deschenes, D. A. Vanden Bout and University of Texas, *Origin 6.0: Scientific Data Analysis and Graphing Software*, Origin Lab Corporation (Formerly Microcal Software, Inc.),

2000, commercial price: 595, academic price: 446, **https://www.originlab.com**.

62 T. Lu and F. Chen, Multiwfn: a multifunctional wavefunction analyzer, *J. Comput. Chem.*, 2012, **33**, 580–592.

63 M. N. Arshad, A.-A. M. Al-Dies, A. M. Asiri, M. Khalid, A. S. Birinji, K. A. Al-Amry and A. A. Braga, Synthesis, crystal structures, spectroscopic and nonlinear optical properties of chalcone derivatives: a combined experimental and theoretical study, *J. Mol. Struct.*, 2017, **1141**, 142–156.

64 M. S. Ahmad, M. Khalid, M. A. Shaheen, M. N. Tahir, M. U. Khan, A. A. C. Braga and H. A. Shad, Synthesis and XRD, FT-IR vibrational, UV-vis, and nonlinear optical exploration of novel tetra substituted imidazole derivatives: a synergistic experimental-computational analysis, *J. Phys. Chem. Solids*, 2018, **115**, 265–276.

65 M. Shahid, M. Salim, M. Khalid, M. N. Tahir, M. U. Khan and A. A. C. Braga, Synthetic, XRD, non-covalent interactions and solvent dependent nonlinear optical studies of Sulfadiazine-Ortho-Vanillin Schiff base: (E)-4-((2-hydroxy-3-methoxy-benzylidene)amino)-N-(pyrimidin-2-yl)benzene-sulfonamide, *J. Mol. Struct.*, 2018, **1161**, 66–75.

66 K. Colladet, M. Nicolas, L. Goris, L. Lutsen and D. Vanderzande, Low-band gap polymers for photovoltaic applications, *Thin Solid Films*, 2004, **451**, 7–11.

67 A. Saeed, S. Muhammad, S. Rehman, S. Bibi, A. G. Al-Sehemi and M. Khalid, Exploring the impact of central core modifications among several push-pull configurations to enhance nonlinear optical response, *J. Mol. Graphics Modell.*, 2020, **100**, 107665.

68 M. Miar, A. Shiroudi, K. Pourshamsian, A. R. Oliaey and F. Hatamjafari, Theoretical investigations on the HOMO–LUMO gap and global reactivity descriptor studies, natural bond orbital, and nucleus-independent chemical shifts analyses of 3-phenylbenzo[d]thiazole-2(3H)-imine and its para-substituted derivatives: solvent and substituent effects, *J. Chem. Res.*, 2021, **45**, 147–158.

69 C.-G. Zhan, J. A. Nichols and D. A. Dixon, Ionization potential, electron affinity, electronegativity, hardness, and electron excitation energy: molecular properties from density functional theory orbital energies, *J. Phys. Chem. A*, 2003, **107**, 4184–4195.

70 R. G. Parr and R. G. Pearson, Absolute hardness: companion parameter to absolute electronegativity, *J. Am. Chem. Soc.*, 1983, **105**, 7512–7516.

71 R. Parthasarathi, V. Subramanian, D. R. Roy and P. K. Chattaraj, Electrophilicity index as a possible descriptor of biological activity, *Bioorg. Med. Chem.*, 2004, **12**, 5533–5543.

72 R. G. Parr, R. A. Donnelly, M. Levy and W. E. Palke, Electronegativity: the density functional viewpoint, *J. Chem. Phys.*, 1978, **68**, 3801–3807.

73 P. Politzer and D. G. Truhlar, *Chemical applications of atomic and molecular electrostatic potentials: reactivity, structure, scattering, and energetics of organic, inorganic, and biological systems*, Springer Science & Business Media, 2013.

74 A. Ali, M. Khalid, K. P. Marrugo, G. M. Kamal, M. Saleem, M. U. Khan, O. Concepción and F. Alexander, Spectroscopic and DFT/TDDFT insights of the novel phosphonate imine compounds, *J. Mol. Struct.*, 2020, **1207**, 127838.

75 M. Khalid, M. U. Khan, R. Hussain, S. Irshad, B. Ali, A. A. C. Braga, M. Imran and A. Hussain, Exploration of second and third order nonlinear optical properties for theoretical framework of organic D–π–D–π–A type compounds, *Opt. Quantum Electron.*, 2021, **53**, 1–19.

76 L. Dalton, M. Lauermann and C. Koos, NLO: Electro-Optic Applications, in *The WSPC Reference on Organic Electronics: Organic Semiconductors. Volume 2: Fundamental Aspects of Materials and Applications*, World Scientific, 2016, pp. 369–396.

77 C. Qin and A. E. Clark, DFT characterization of the optical and redox properties of natural pigments relevant to dye-sensitized solar cells, *Chem. Phys. Lett.*, 2007, **438**, 26–30.

78 P. N. Prasad and D. J. Williams, *Introduction to nonlinear optical effects in molecules and polymers*, Wiley, New York, 1991.

79 M. Khalid, R. Jawaria, M. U. Khan, A. A. C. Braga, Z. Shafiq, M. Imran, H. M. A. Zafar and A. Irfan, An efficient synthesis, spectroscopic characterization, and optical nonlinearity response of novel salicylaldehyde thiosemicarbazone derivatives, *ACS Omega*, 2021, **6**, 16058–16065.

80 D. R. Kanis, M. A. Ratner and T. J. Marks, Design and construction of molecular assemblies with large second-order optical nonlinearities. Quantum chemical aspects, *Chem. Rev.*, 1994, **94**, 195–242.